Dissecting Earth's Magnetosphere: 3D Energy Transport in a Simulation of a Real Storm Event

A. Brenner[1,2], T. I. Pulkkinen[1], Q. Al Shidi [1], G. Toth [1]

[1]University of Michigan Climate and Space Sciences and Engineering Department
[2]University of Michigan Aerospace Engineering Department

Key Points:

- Simulation results are used to quantify the global energy dynamics of Earth's magneotsphere in terms of energy pathways.
- Externally during main phase 61 PJ of energy is lost from the closed region due to erosion while 92 PJ of energy enters the lobe region.
- Internally, 70PJ of energy is recirculated at the cusp from the closed to open field, then passed back to the closed region in the tail.

Corresponding author: Austin Brenner, `aubr@umich.edu`

Abstract

We present new analysis methods of 3D MHD output data from the Space Weather Modeling Framework during a simulated storm event. Earth's magnetosphere is identified in the simulation domain and divided based on magnetic topology and the bounding magnetopause definition. Volume energy contents and surface energy fluxes are analyzed for each subregion to track the energy transport in the system as the driving solar wind conditions change. Two energy pathways are revealed, one external and one internal. The external pathway between the magnetosheath and magnetosphere has magnetic energy flux entering the lobes and escaping through the closed field region and is consistent with previous work and theory. The internal pathway, which has never been studied in this manner, reveals magnetically dominated energy recirculating between open and closed field lines. The energy enters the lobes across the dayside magnetospheric cusps and escapes the lobes through the nightside plasmasheet boundary layer. This internal circulation directly controls the energy content in the lobes and the partitioning of the total energy between lobes and closed field line regions. Qualitative analysis of four-field junction neighborhoods indicate the internal circulation pathway is controlled via the reconnection X-line(s), and by extension, the IMF orientation. These results allow us to make clear and quantifiable arguments about the energy dynamics of Earth's magnetosphere, and the role of the lobes as an expandable reservoir that cannot retain energy for long periods of time but can grow and shrink in energy content due to mismatch between incoming and outgoing energy flux.

Plain Language Summary

Results of computer simulation of near Earth space is looked at in a new way to understand how energy moves around the global system. It is found that in addition to a pathway of energy from the outside into the system and back again there is an internal loop which recirculates energy. These new methods will greatly improve our understanding how the whole magnetosphere system evolves and will help address evolution of processes that have space weather impacts.

1 Introduction

Energy that couples from the solar wind into Earth's magnetosphere can have significant negative consequences on terrestrial life. Global dynamics of energy within Earth's magnetosphere has long been a topic of interest since original works by Dungey (1961), who presented a clear combination of events involving dayside magnetic reconnection, advection of opened field lines and a re-closing of field lines at a tail reconnection site. Twenty years later, Akasofu (1981) presented a quantified picture of energy balance within the magnetosphere. In this work it was hypothesized and evidence was found for a system in which energy input from the solar wind was fully consumed by a combination of the enhancing ring current, Joule heating in the ionosphere, and precipitating auroral flux. Notably any plasma or magnetic energy contained in the open flux lobes was omitted, which would seem to suggest that the tail reconnection process would not significantly impact the energy balance, because that energy flows through the lobes without being stored there. We now have simulation tools to take a new look at this energy balance hypothesis and dig deeper into the energy transfer between sources and their specific timings.

In the following decade the International Solar-Terrestrial Physics program released the first Inter-Agency Consultative Group campaign with an objective to define "the structure and energy flow through the boundary layers of the Earth's magnetosphere"(Mish et al., 1995). Many publications and valuable data sets resulted from this program, but as of yet there has not been a comprehensive quantitative resolution of this objective. This is because it is difficult to extrapolate observed pointwise boundary crossings to determine the full surface geometry, and field values on the geometry to obtain integrated energy flux. It remains an open question how exactly energy circulates through the various boundaries in the magnetosphere system.

Global energy dynamics in the magnetosphere have been studied using simulation as far as the magnetopause boundary. Palmroth et al. (2003) and Pulkkinen (2007) showed the dependence of clock angle on the amount of energy and energy content through the magnetopause. Hoilijoki et al. (2014), Lu et al. (2021), H. Zhang et al. (2023) have also shown that the type of energy entering the system varies significantly with the radial component of the interplanetary magnetic field (IMF) and the dipole tilt. Brenner et al. (2021) took this a step further showing the energy flux through a full magnetopause surface including a bounding tail cutoff and a forward surface. By using the magnetic field rather than the flow field to construct the magnetopause surface, it was shown that the effect of magnetic reconnection on the dayside results in energy outflow in the form of hydrodynamic flux at $X_{GSM} > 0$ and Poynting flux inflow at $X_{GSM} < 0$. These dynamics were also seen in a study by Ala-Lahti et al. (2022) using a 2D version of the Vlasiator code (Palmroth et al., 2018). This is in contrast with previous studies by Lu et al. and H. Zhang et al. who conclude that hydrodynamic flux (there referred to as mechanical energy flux) is entering the system near the magnetopause nose. The difference arises from their choice of the magnetopause boundary definition. We argue that the magnetopause definition outlined in this paper is the best choice when considering the energy circulation between the solar wind and the magnetosphere and within the magnetosphere – ionosphere system.

The internal workings of the magnetosphere, namely the energy transport within the system, has not been studied in detail using global simulation explicitly. However, there have been many important works which provide insight into how the system is expected to behave. Many studies have shown that the IMF clock angle has direct control of how the magnetosphere opens and allows solar wind plasma to enter the system. Specifically, studies using observations from the Cluster mission have shown how the magnetic cusp responds to a change in the reconnection line position causing a reversal of the reconnection outflow relative to the open-closed field line boundary (Escoubet et al., 1989; Lavraud et al., 2005) (see also recent review of magnetospheric cusp findings from the Cluster mission by Pitout et al. (2021)). When the IMF is northward and high latitude reconnection occurs, the energy transport is not captured in the coupling functions such as the Newell et al. (2007) function, while it is thought to be one possible mechanism for energy influx. Specifically this may result in energy influx when both north and south lobes reconnect simultaenously, known as dual lobe reconnection (Russell, 1972). Milan et al. (2020) summarizes the various possibilities of reconnection between the sheath and open-closed field lines, and shows evidence for dual lobe reconnection signatures in the ionosphere. Finally, Glocer et al. (2020) show simulation results on how the magnetosphere may be largely populated by ions coming from polar wind outflow rather than from the solar wind, highlighting the significant role the inner boundary must also play in the energy transport. Although we do not employ a two-way coupled polar wind outflow model in this study, the effective mass transport out of the system due to the fixed density inner boundary condition mimics real outflow effects (Welling & Liemohn, 2014).

In this work, we use results from a coupled global space environment simulation to address the following questions:

1. What is the energy balance in the magnetosphere during a real storm event? What determines the energy split between open and closed field line regions and what conditions internally and externally cause it to change?
2. What is the energy pathway between the magnetosphere and surrounding (shocked) solar wind plasma? In contrast, what are the energy pathways internal to the mag-

netosphere? How do each of these respond to variations in the external solar wind and IMF conditions and internal system state?

2 Space Weather Modeling Framework (SWMF)

In this work, we use the Space Weather Modeling Framework (SWMF) in the Geospace configuration (Toth et al., 2012). This configuration includes the BATS-R-US in ideal MHD mode for the Global Magnetosphere, Ridley Ionosphere Model (RIM) for Ionosphere Electrodynamics, and the Rice Convection Model for the Inner Magnetosphere. The MHD domain was configured with 1/2 R_E grid resolution inside a paraboloid aligned with the X_{gsm} direction with height of 52 R_E and a radius of 35 R_E at the base ranging from +20 to -32 R_E to capture the extent of the magnetopause. Additionally, within a box $-20 < X < 8$ and $-8 < Y, Z < 8$ and in X the resolution was increased to 1/4 R_E. Finally in a spherical shell from the inner boundary of 2.5 R_E out to 8 R_E the resolution was increased again to 1/8 R_E (see Figure 1). The ionosphere model included the Conductance Model for Extreme Events (CMEE) (Mukhopadhyay et al., 2020).

3 Observations

The event selected for this study is the well-known Starlink event in which 38 commercial satellites launched as part of the Starlink constellation were lost due to thermospheric upwelling (Zhang et al., 2022). It is a recent event, which allows us to take advantage of the growing number of Earth-orbiting space missions. Figure 2 shows comparisons of observed and simulated geomagnetic indices, demonstrating the suitability of the simulation for capturing the global scale physics.

The ground-based observations can be used for comparison with the simulation results. The third panel of Figure 2 shows the Sym-H index constructed from a series of mid to low latitude magnetometer station recordings, typically responding to the variations in the ring current encircling the Earth within the inner magnetosphere. While the magnitude is somewhat off especially during the recovery phase of the storm, the overall temporal evolution is well captured by the simulation. We define the storm main phase as the rapidly decreasing Sym-H period, ending at the peak value of the observed Sym-H.

The Supermag SML index (Gjerloev, 2012) (bottom panel of Figure 2) is constructed using high-latitude magnetometer records responding mostly to ionospheric currents and auroral activity. To make a 1-1 comparison to the SML index, we seed virtual magnetometers for each point in the Supermag network in the simulation domain and compute the northward component of dB. The minimum dB_n value from the high latitude subset of stations is taken as the simulated SML index value. Consistent with recent work by Shidi et al. (2022), who showed that SWMF has a lower average Heidke Skill Score for high latitude magnetic disturbance predictions, the simulation does not capture the very high auroral currents that were observed during the main phase of the storm.

We use the Cluster-1, Magnetospheric Multiscale (MMS) 1, and Time History of Events and Macroscale Interactions during Substorms (THEMIS) A, D, and E spacecraft to compare in-situ plasma and magnetic field measurements with the simulation results. The orbits are shown in Figure 3 with contours of the virtual status variable which represents the topological region of the magnetosphere within which the virtual satellite was in at that time. As evident in the plots, the orbits include magnetopause boundary crossings as well as crossings between open and closed field lines, which allow us to compare the observed crossings with the simulation boundary locations.

Figure 4a shows the comparison of the z component of the magnetic field at the locations of the THEMIS, Cluster, and MMS spacecraft. In the magnetosphere, the B_z

component is a good proxy for the magnetic energy density in the system, while also capturing the sign change associated with leaving the magnetosphere during southward IMF. On the same plot, on the right vertical axis, we plot the magnitude of the local Poynting flux $|\mathbf{S}|$. This derived quantity is constructed from the local magnetic field strength and bulk velocity, as discussed in more detail below (see Equation 2). While the B_z is a useful proxy, the Poynting flux is a direct measure of the electromagnetic energy transport, and therefore a key quantity for the purpose of this paper. Similarly, Figure 4b shows the observed and simulated total pressure P on the left axis and the local magnitude of hydrodynamic flux $|\mathbf{H}|$ on the right axis (see Equation 1 and discussion below).

Overall the differences in the magnitude of the state variables (B_z,P) as well as the derived flux magnitudes ($|\mathbf{S}|$, $|\mathbf{H}|$) are similar. The data – model comparison results are discussed further in Section 5.4.

4 Methods

4.1 Region Identification

In order to analyze the energy transport within the 3D MHD output domain, the energy density must be integrated over a volume and energy flux through a surface. While the choice of the volume(s) and surface(s) can be arbitrary, we select definitions that distinguish physically significant boundaries that separate plasmas with different properties, while keeping the analysis concise with objects that are clearly defined and limited in number.

Building on previous work by Brenner et al. (2021) we first define the magnetopause, which sets the boundaries of the magnetosphere. The magnetopause definition uses a combination of the field line tracing status variable for closed field lines with the modified plasma-beta $\beta^* = 2\mu_0(P_{th} + P_{dyn})/B^2$, which was first introduced in a study of the Martian magnetosphere (Xu et al., 2016). The β^* limit chosen was 0.7, but the sharp gradients in this variable result in a very forgiving choice in the limit value close to unity. To account for cases when the solar wind β^* value dips below the limit value, we add the condition that solar wind field lines are explicitly omitted. (Note that this also omits plasma tailward of the distant X line, if it reaches within the X_{gsm} cutoff. This plasma tends to be high β^* and traveling away from the Earth.) The X_{gsm} cutoff is set at $X = -20R_e$, and the inner boundary (of the analysis, not the simulation domain) is set at $r = 4R_e$, close to where the MHD model is coupled to the ionospheric electrodynamics model ($3R_e$). Below this altitude, there may be numerical boundary effects which make the analysis results less accurate and meaningful. This definition captures the spatial region where the plasma is dominated by the planet's magnetic field, and thus forms a strong definition for the magnetosphere.

Once the magnetosphere system volume is identified, further subclassification is done in order to track energy within the system. To keep the analysis limited and the boundaries well defined, we make only two splits: The first is the open-closed field line boundary. This separates the open flux lobes from the closed field line region of the magnetosphere. The plasma in the closed field line region experiences different physics than the open field line plasma: In the inner magnetosphere, the particle drifts separate ion and electron motions, which in the simulation is captured by coupling the MHD code with a drift kinetic code, the Rice Convection Model. The open closed boundary is easily determined using the status variable, and, as discussed above, separates distinct plasma populations.

The second split is done based on day-night magnetic field mapping. Since, by definition, the entire magnetosphere system is magnetically connected to the inner boundary ionosphere, we can divide the volume to regions mapping to the dayside and nightside (with respect to the magnetic terminator plane), respectively, without loss of volume or creation of additional unclassified volumes. This division is simply implemented by assigning the magnetically mapped north and south footpoint coordinates to each point in the 3D GM domain. Using the x coordinate of the footpoint, we can separate the dayside magnetospheric cusp boundary from the nightside plasmasheet boundary layer, that may exhibit different energy transport phenomena.

The two core quantities we examine are the energy density integrated over a volume and the energy flux integrated over a surface. The volumes of interest are limited to the lobes and closed regions, as well as their sum, which makes up the total magnetosphere. The surface flux analysis, however, is detailed to cover the integrated flux across each interface of the magnetospheric system. With these definitions, there are six distinct regions that any point in the domain can belong to: I. outside magnetosphere, II. dayside lobes, III. nightside lobes, IV. dayside closed, V. nightside closed, VI. inside inner boundary (see Figure 5a). The interfaces between each of these 6 regions results in a number of integrated flux values, the most relevant of which are explored in this paper (see arrows and numbered boundaries in Figure 5a).

4.2 Energy Transport Integration

In discussing both the volumetric energy contents and surface energy fluxes, we evaluate the hydrodynamic energy (and its flux) and the magnetic energy (and the Poynting flux) separately; together they make up the total energy and flux quantities. The hydrodynamic energy flux **H** and Poynting flux **S** can be written in the form

$$\mathbf{H} = \left(\frac{1}{2}\rho u^2 + \frac{\gamma}{\gamma-1}P_{th}\right)\mathbf{u} \tag{1}$$

$$\mathbf{S} = \frac{B^2}{\mu_0}\mathbf{u} - \frac{\mathbf{B}\cdot\mathbf{u}}{\mu_0}\mathbf{B} \tag{2}$$

where ρ is mass density, $\mathbf{u}$ is the MHD bulk velocity, P_{th} is plasma thermal pressure, $\mathbf{B}$ is the magnetic field, and γ is the ratio of specific heats. Together, these sum to the total energy flux $\mathbf{K} = \mathbf{H} + \mathbf{S}$.

Similarly, the total energy density U is split into hydrodynamic (U_{P0}) and magnetic (U_B) components, which allows us to write the total energy flux and energy content equations as

$$\mathbf{K} = \mathbf{H} + \mathbf{S} = \left(\frac{1}{2}\rho u^2 + \frac{\gamma}{\gamma-1}P_{th} + \frac{B^2}{\mu_0}\right)\mathbf{u} - \frac{\mathbf{B}\cdot\mathbf{u}}{\mu_0}\mathbf{B} \tag{3}$$

$$U = U_{P0} + U_B = \left(\frac{1}{2}\rho u^2 + \frac{P_{th}}{\gamma-1}\right) + \frac{B^2}{2\mu_0} \tag{4}$$

This split into hydrodynamic and magnetic energy components is included to allow investigation of the physical mechanisms that may drive energy transport at the various boundaries. The goal of this methodology is to keep the analysis comprehensive while also clear and limited in scope.

Finally, it is important to track both the static and motional contributions of flux through a surface that can move between two timesteps. As defined in Brenner et al. (2021), we include the motional component of all energy flux values by tracking the volumes traded between the 6 regions between each pair of consecutive time steps. This flux contribution from the moving surface can be approximated by

$$\int_{\mathcal{S}(t)} U\mathbf{q}\cdot\mathbf{d}\mathcal{S} = \int_{d\mathcal{V}/dt} Ud\mathcal{V} \approx \frac{1}{\delta t}\int_{\delta\mathcal{V}} Ud\mathcal{V} \tag{5}$$

where $\mathcal{S}$ indicates a 2D surface in 3D space moving with velocity $\mathbf{q}$, $\mathcal{V}$ indicates the enclosed 3D volume and $\delta\mathcal{V}$ is the volume covered by the moving surface in time δt. For example, if a small volume of the dayside magnetosphere was in the dayside closed region at time t_0 and at time $t_1 = t_0 + \delta t$ is now outside the magnetosphere, the energy contained in that small volume is considered as an energy flux from the closed region to the magnetosheath over a time period of δt. This is illustrated in Figure 5b.

5 Results

5.1 Volumetric Energy

Figure 6 shows the total volume integrated energy in regions of the magnetosphere stacked so that the top line represents the full magnetosphere volume. The main phase of the storm shown in the grey shaded region clearly shows the total energy increase followed by a slower energy decay as the system recovers. Comparing this with the Sym-H index in Figure 2 shows how good a proxy it is for the total energy content in the magnetosphere.

Figure 6 also shows how variable the energy partitioning is between the closed and open field regions: The volume energy rate of change indicated by the slope of the stack interface is much stronger than the rate of change of the total. In order to understand what's happening between the two regions we next examine the variation in the surface energy flux values.

5.2 Surface Flux

Figure 7 summarizes the energy flux across the external regional interfaces which includes both the instantaneous energy flux across the static interface as well as the energy flux due to surface motion. The magnetopause surface is broken down into four sections: interface 1 between the lobes and the magnetosheath, interface 5 between the closed region and sheath, interface 4 between the lobes and the exterior through the tail cutoff, and interface 6 between the closed region and the exterior through the tail cutoff. Likewise, the inner boundary is split into two sections: interface 3 toward the open field and interface 7 toward the closed field each at a fixed distance of $4R_e$ from the Earth's center (see surface definitions and reference vectors shown in Figure 5a).

The three panels of Figure 7 show the exchange of hydrodynamic energy, Poynting flux, and total energy flux, respectively. The sign convention for the flux calculation is with the surface normal pointing away from the interior of the reference volume so that positive values indicate energy escaping the system. From the top panel we see that kinetic and thermal energy is escaping via the closed region throughout main phase, followed by a shortlived reversal in the average that seems to follow the IMF B_z turning briefly northward then back southward.

The middle panel shows that Poynting flux through the lobe – sheath interface dominates the total, and that this energy is going into the magnetosphere. For the Poynting flux, there are more contributors as well during the main phase as later during the recovery. Magnetic energy transport out from the inner boundary to the open flux tail lobes represents low density, cold plasma outflow from the strong dipole magnetic field. This energy inflow is countered by the magnetic energy transferred out from the system through the inner boundary surface toward the closed field region. These two flux contributions appear to be quite balanced, but the lobe inner boundary flux steadily increases then decreases, while the closed inner boundary flux seems to retain a constant rate throughout most of the main phase.

The bottom panel showing the total energy transfer depicts the sum of the above results with only the lobe magnetosheath number 1 interface changing sign between integrated **H**, **S**, and **K**. This can be explained by looking at the form of the equations and noting that in the motional case they cannot differ, and the static case all energy is transported with the velocity except for the $(-\mathbf{B}\cdot\mathbf{u})\,\mathbf{B}/\mu_0$ portion of the Poynting flux. This means that this transport along the magnetic field direction rather than the flow field direction is dominating the flux between the sheath and lobes.

Figure 8 summarizes the energy flux across the internal interfaces in the magnetosphere system, the flux sign is now with respect to the closed region so that positive flux transfers energy from the closed regions to the open tail lobes. The top panel reveals that there is very little hydrodynamic energy exchanged at the dayside cusp (integrated H_{2a}) or tail plasmasheet boundary layer (integrated H_{2b}) with a slight bias to energy moving through the cusp toward the lobes.

The middle panel shows very large integrated Poynting fluxes, especially during the main phase, with maximum magnitudes approaching double that of the external fluxes. The balance is also now reversed with the tail interface (integrated S_{2b}) dominating the sum at almost all times. The connection of the temporal evolution with the IMF clock angle is apparent as there is a clear drop in both internal integrated Poynting fluxes before the end of the main phase. Especially, the cusp flux reverses sharply right at the end of main phase.

The total integrated energy flux for the internal interfaces is almost entirely in the form of Poynting flux, and is much larger in magnitude than the external energy fluxes. This indicates that magnetic energy is recirculating in the system via slow, cold, low density plasma with high magnetic field strength embedded within it.

Table 1 compares the various spatially integrated surface flux values by integrating the power contribution in time over the main phase interval to obtain a total energy exchange through each interface. The signs of the values are consistent with the spatially integrated flux timeseries plots. This tabular format highlights the large amount of energy moving through the internal interfaces 2a (dayside closed field region to tail lobes) and 2b (night-side closed field region to tail lobes). To further demonstrate this internal energy re-circulation, we add up the energy entering through 1 (tail lobes to magnetosheath) and the energy returned through 2a (closed field region to the lobes) that amounts to 163 PJ, which is close to the energy transferred through boundary 2b from the lobes to the closed field region in the tail of 157 PJ. This suggests that a large portion of the energy acquired by the lobes from the magnetosheath is transmitted to the closed field region and sent right back to the lobes in a recirculating loop. Note that when performing integrations over both space and time for an 8 hour window such as this, even small biased errors in the surface flux can result in large changes in the total energy transported. Care was taken to avoid spurious effects from the inner boundary, and relative magnitude values for the largest fluxes were unaffected by these changes.

5.3 Reconnection lines

Figure 9 examines the locations of potential reconnection sites in relation to the magnetopause field topology. The four field junction (Laitinen et al., 2007) represents the location where four magnetic topologies (closed-closed, open-closed, closed-open, open-open) are all adjacent to each other and indicates the possibility of magnetic reconnection. The figure shows the neighborhood of four field junction cells (green), in reference to the magnetopause color coded with the magnetic connecivity status variable from two different viewing angles.

The first panel shows the rapid evolution of the system starting from the moment of B_z reversal at the end of main phase and then progressing in 10-minute increments. The magnetospheric cusp is also indicated in this figure as the dayside mapped boundary between open and closed field. Considering that reconnection has to happen near the four field junction neighborhoods, the Figure demonstrates how the northward turning IMF first splits the single dayside X line, then the split X-line advects and is replaced by an additional split X-line that covers large sections of both the closed and open magnetopause. From the color coding showing open and closed field it is clear that dual lobe reconnection is occurring, as the lighter color closed region quickly expands to cover most of the shown magnetopause surface. These snapshots are taken from an animated video (see supplementary material), which demonstrates the explosive nature of the changing reconnection pattern.

5.4 Data Model Comparison

The right axes of Figures 4a and 4b show the satellite trace comparison of the magnitude of Poynting and hydrodynamic energy flux $|\mathbf{S}|$ and $|\mathbf{H}|$. For the Cluster 4 satellite, the simulated and observed flux magnitudes match well, especially during the main phase. There is a noticeable discrepancy just after the main phase ends, when the observed hydrodynamic energy flux is much larger than the energy flux predicted by the simulation.

Observations of all three THEMIS probes show two intervals when the satellite is crossing through a magnetospheric boundary. The first between -16:30 hours and -14:00 hours when probes A and E initially reside in the open tail lobes as both the closed field region and the magnetosheath pass over several times. Probe D, just a small distance away, spends its time mostly in the closed field region during this time. All three probes have similar trends between the observed and simulated flux values, with the observed Poynting flux having more variations and a higher average value. Probe D within the closed field region also shows much lower hydrodynamic energy flux than those predicted by the simulation.

The next interval of crossings occurs during the main phase (between –8 hours and 0 hours). Both the closed field region to lobe boundary and the tail lobe to magnetosheath boundary pass over each of the THEMIS satellites between -4:00 hours and -2:30 hours. For these crossings, the observed energy flux magnitude split does not agree with the simulation results: The simulated values predict too much hydrodynamic energy flux and too little Poynting flux. Looking into the detailed components, specifically the simulation B_z magnitude drops where the observed field does not. This indicates reconnection transporting flux away from the magnetopause boundary in the simulation that is not happening to the same degree in the observations.

Finally, the MMS1 probe is compared with the simulation data (the inter-spacecraft spacing is too close to be resolved by the simulation grid size, so only one probe is used as a point comparison). Between –12:30 hours and –11:00 hours, MMS1 is near the magnetopause. Comparison with the simulation values shows a much better agreement in the Poynting flux than in the hydrodynamic flux. The observed hydrodynamic flux magnitude peaks at much higher values, and after this point maintains a constant difference to the simulated values. During the main phase between –3:00 hours and –1:00 hours, there are enhancements in the observed B_z that are entirely missed by the simulation. These transients may be caused by smaller-scale structures in the magnetosheath, or transient perturbations either at the bow shock or at the magnetopause.

5.5 Interpretation

Taking the individual results together, we see an emerging picture of two distinct energy pathways and an apparent mode shift. Energy exhange through the magnetosphere's external boundaries follows the classic Dungey cycle, but instead of focusing only on magnetic flux (as the Dungey cycle does), we consider the total energy circulation. Energy is lost from the dayside closed field region as it opens through dayside reconnection; this is recorded as integrated hydrodynamic energy loss from the system through the H5 boundary (from dayside closed field line region to the magnetosheath) during main phase. Simultaneously, magnetic energy in the newly opened field is drawn back into the system through the lobes. This is what is recorded as the integrated Poynting flux injection through S1 boundary from the magnetosheath into the open lobes. The results clearly show that these two interfaces dominate the energy flux transport. As the latter is a source and the former is a sink, the result demonstrates how the magnetosphere simply captures a portion of energy coming from the solar wind: During the main phase, both the escape and injection increase, and it is only the imbalance that increases the system's total energy.

Detailed examination of the energy distribution between the open and closed field line regions reveals a significant amount of recirculating Poynting flux, which comes into the closed region through the tail (boundary 2b from the tail lobe into the nightside plasma sheet) and returns almost as much through the cusp interface (boundary 2a from dayside closed field region to the open field region). This explains why the closed field line energy is decreasing during main phase, while the lobe energy content and total magnetospheric energy content are increasing.

It would seem that the closed field region is not able to trap all the (electromagnetic) energy generated by the flux erosion on the dayside. While plasma cannot be confined in the open flux lobes, the results demonstrate how the open flux region can accumulate and store energy by setting up this recirculation pattern. During the storm main phase, the volume and energy of the lobes grow, despite exchanging vast amounts of energy at both ends.

To understand the dynamics at the end of main phase (time T=0 hours), we put several clues together. First, energy in the lobes is rapidly lost while the closed region energy rapidly increases. While the total energy does increase, the change mostly appears as a transport of energy from the lobes to the closed region (see stack plot in Figure 6). Qualitative results of the 3D magnetopause surface with the four field junction neighborhoods displayed (see Figure 9) show the potential reconnection locations wash over large regions of the open flux lobes, and later those sections changing topology to closed field. The only way for the open lobes to become closed in this way is for reconnection to occur on both north and south lobes, i.e., dual lobe reconnection is taking place.

Examination of the internal energy flux results at that moment shows that the direction of flux reverses, as energy flows from the lobes to the dayside closed field just after the main phase end. While the signs of dual lobe reconnection are clear in the simulation results, unfortunately the satellites were not well positioned during the end of the main phase to record that phenomenon. However, THEMIS crossings earlier in the main phase suggest that the simulation overpredicts the rate of reconnection as evidenced by overabundance of thermal and kinetic energy and missing closed magnetic flux. This may mean that the amount of dual lobe reconnection seen in the simulation is overpredicted and warrants further investigation.

Finally, we discuss how the solar wind driving relates to the energy dynamics. Clearly both the external and internal energy pathways show a difference between the main phase and recovery phase as the IMF B_z component rotates away from due southward orientation. For the external energy flux values, the sharp decline does not occur until both the IMF B_z and B_y magnitudes drop, which is confirms that it is the clock angle that is important to the solar wind – magnetosphere coupling rather than the IMF B_z alone. However, for the internal energy transport, the energy flux sharply decreases about 90 minutes earlier, which does correspond to the decrease in IMF B_z. This would seem to indicate that the internal circulation loop is more strongly associated with B_z rather than the IMF clock angle. The different responses of the system highlight the complexity of the dynamics and hence the difficulty in devising universal coupling parameters targeted to predict the system state.

6 Discussion

Our results depict a different picture of energy storage in the magnetosphere system from that of Akasofu (1981). In particular, we note that energy is indeed stored in the tail lobes in electromagnetic form, by increasing the magnetic field strength in the lobes. This energy accumulation is realized as a recirculation pattern where the energy in the lobes is transferred from the dayside closed region to the nightside tail region, and as more energy is added to the system, the boundaries of the lobes expand and the field magnitude increases to accommodate the increased energy content.

Another way to illustrate the magnetic energy input and recirculation within the magnetosphere is using the language of basic circuit elements (see e.g. Mays et al. (2009), who have taken this approach to a fully fledged model). In this representation, the lobes act as a combination of inductors and capacitors which store and release magnetic energy via the magnetopause, tail, and Region 1 currents, which are all connected and driven by the solar wind electric potential. Because the energy transported through the lobes is almost entirely magnetic, this analogue provides a good illustration of how the energy dynamics work in that region.

Moving from the energy storage to the energy transport, the cusp plays a key role in determining the internal magnetospheric transport. In a previous study of the cusp using Cluster observations, Pitout et al. (2021) argue that motion of the reconnection line across the cusp should reverse the flux transport between open and closed field lines. Our results indicate that this trend indeed holds in that the energy transport between dayside lobes and closed region reverses, although the actual dynamics of the reconnection line appear to be much more complex than that represented by a two-dimensional cartoon.

Considering these global magnetosphere dynamics from the ionospheric perspective, our results are consistent with the Expanding Contracting Polar Cap (ECPC) theory (Lockwood et al., 1992). In this theory, the polar cap boundary is formed as an unsteady superposition of dayside flux expansion with the nightside flux contraction, and the rest of the polar cap boundary expands along the adiaroic (Siscoe & Huang, 1985) boundary. This simultaneous expansion and contraction of magnetic flux is exactly the same as re-circulation of magnetic energy through the system presented here (see Figure 10). Future work to merge the ionospheric results with the magnetospheric dynamics presented here can bridge the difference in terminology and solidly quantify magnetosphere-ionosphere coupling in terms of energy and magnetic flux transport.

The internal circulation pathway seen in our results can be directly linked to cold dense material from the plasmasphere being recirculated up and over the poles. This scenario presented by Freeman et al. (1977) demonstrates the same pathway that the magnetic energy would flow; $\mathbf{E}\times\mathbf{B}$ corresponds to both plasma drift motion and magnetic energy flux. In other words, the slow cold plasma with strong magnetic field frozen in moves across the poles and recirculates sunward in the closed field region. A more recent study by Christian-Andrew Bagby-Wright et al. (2023) using a coupled plasmasphere model demonstrates how this effect would also evolve throughout a storm. In this work, without the coupled multi-fluid model, the recirculation plasma should have much lower densities. Adding a plasmasphere model could change both the magnitude and timing of the recirculation energy.

A large part of the cusp energy dynamics seen here is connected to dual lobe reconnection happening in the simulation. Imber et al. (2007) have shown observational evidence of such phenomenon occurring when the IMF $B_z > 0$ and clock angle is close to zero (due northward IMF), which is what we observe at the end of the main phase of the Starlink storm studied here. However, based on the limited observations available for this event, it is likely that the simulation is overpredicting the scale and widespread nature of reconnection, which leads to more dual lobe reconnection than occurred in reality.

There are many ways available to adjust reconnection physics in the simulation. First, in the ideal MHD framework, the reconnection rate is determined by the numerical diffusion of the magnetic field, which is affected by the grid size as well as the choice of numerical implementation including the scheme, limiter, speed of light adjustment factor, etc. (Ridley et al., 2010). Second, other physics can be included by changing the MHD equations to include more terms (Hall or resistive MHD) or including a coupled particle in cell model (Chen et al., 2017) in limited regions of the simulation. Importantly, this work demonstrates the capability to quantify the energy dynamics processes, which will enable future studies using these tools to probe the connection between the kinetic reconnection physics and the global energy transport.

7 Conclusion

In this study the Space Weather Modeling Framework (SWMF) was used in the Geospace configuration to simulate Earth's magnetosphere for a storm event on February 3, 2022 (the Starlink event). The energy transport was examined by identifying two distinct volumetric regions and several surface interfaces. Consistent with previous work, we found that kinetic and thermal energy escapes the dayside closed field region, and magnetic energy is injected through the lobes during storm main phase. At the same time, an internal recirculation pattern is set up that transfers magnetic flux from the lobes to the closed field region in the nightside and back from the closed field to the open lobes through the dayside cusp region.

At the end of the main phase, the simulated magnetosphere undergoes dual lobe reconnection which rapidly depletes the magnetic energy flowing through the lobes while adding net energy to the system. However, satellite observations and the Sym-H index indicate differences between the simulation and observed values at that time, which may indicate that the model is not capturing the true dynamics of the system. This may act as evidence of the effects of kinetic scale physics on the global energy dynamics, highlighting the need to resolve the small scale physics in order to be able to quantify the large scale effects.

Returning to the questions posed in the introduction, we conclude the following:

1. The open magnetotail lobes play a critical role in the energy balance in the magnetosphere during storm times. The total magnetospheric energy distribution between the lobes and the closed field region is determined by how much energy is allowed to recirculate from the dayside closed region into the lobes under southward IMF conditions. This energy transfer rate is controlled by the IMF B_z.
2. External energy exchange at the magnetopause is found to be consistent with previous studies, with plasma energy flowing out through the dayside magnetopause and Poynting flux entering through the nightside magnetopause. The latter process is controlled by the IMF clock angle $\theta = \tan^{-1}(B_y/B_z)$. Internal magnetic energy transits from the lobes directly into the nightside closed region, and a portion of that energy is circulated back into the lobes through the cusps on the dayside. The cusp dynamics ultimately thereby determine the internal energy circulation.

8 Open Research

- The simulation output data used for calculating magnetosphere energy transport in this study are available at [Deep Blue Repository Setup in Progress] via [DOI TBD] with [license, access conditions]

- Version 9.90 of the Space Weather Modeling Framework is used for simulating geospace. Access to the full SWMF requires user registration and signing the user license agreement. An open source version is preserved at https://github.com/MSTEM-QUDA/SWMF. The open source version of the SWMF is the Michigan Sun-to-Earth Model with Quantified Uncertainty and Data Assimilation (MSTEM-QUDA distributed under a non-commercial license), for more information about the user liscense agreement and the open source version see http://csem.engin.umich.edu/tools/swmf/.

Acknowledgments

We gratefully acknowledge the SuperMAG collaborators (https://supermag.jhuapl.edu/info/?page=acknowledgem

References

Akasofu, S. (1981). Energy coupling between the solar wind and the magnetosphere. *Space Sci. Rev.*, *28*, 121–190.

Ala-Lahti, M., Pulkkinen, T. I., Pfau-Kempf, Y., Grandin, M., & Palmroth, M. (2022). Energy flux through the magnetopause during flux transfer events in hybrid-vlasov 2d simulations. *Geophysical Research Letters*, *49*(19), e2022GL100079. Retrieved from `https://agupubs.onlinelibrary.wiley.com/doi/abs/10.1029/2022GL100079` (e2022GL100079 2022GL100079) doi: https://doi.org/10.1029/2022GL100079

Brenner, A., Pulkkinen, T. I., Al Shidi, Q., & Toth, G. (2021). Stormtime energetics: Energy transport across the magnetopause in a global mhd simulation. *Frontiers in Astronomy and Space Sciences*, *8*. Retrieved from `https://www.frontiersin.org/articles/10.3389/fspas.2021.756732` doi: 10.3389/fspas.2021.756732

Chen, Y., Toth, G., Cassak, P., Jia, X., Gombosi, T. I., Slavin, J. A., … Henderson, M. G. (2017). Global three dimensional simulation of earth s dayside reconnection using a two way coupled magnetohydrodynamics with embedded particle in cell model initial results 3 d mhd epic simulation of magnetosphere. *Journal of Geophysical Research*. doi: 10.1002/2017ja024186

Christian-Andrew Bagby-Wright, D. Welling, R. Lopez, R. Katus, & B. Walsh. (2023). Recirculation of plasmasphere material during idealized magnetic storms. *Frontiers of Physics*. (S2ID: ef32f92cd7e857d80a5def384e81afd3934fb052) doi: 10.3389/fphy.2023.1146035

Dungey, J. W. (1961, Jan). Interplanetary magnetic field and the auroral zones. *Phys. Rev. Lett.*, *6*, 47–48. Retrieved from `https://link.aps.org/doi/10.1103/PhysRevLett.6.47` doi: 10.1103/PhysRevLett.6.47

Escoubet, C., J.M Bosqued, & Bosqued, J.-M. (1989, May). The influence of IMF-Bz and/or AE on the polar cusp: An overview of observations from the AUREOL-3 satellite. *Planetary and Space Science*, *37*(5), 609–626. (MAG ID: 2017772289) doi: 10.1016/0032-0633(89)90100-1

Freeman, J. W., Hills, H. K., Hill, T. W., Reiff, P. H., & Hardy, D. A. (1977, May). Heavy ion circulation in the Earth's magnetosphere. *Geophysical Research Letters*, *4*(5), 195–197. (MAG ID: 1986391739 S2ID: 8926eee5f423154d3d84286694c9212d9b289671) doi: 10.1029/gl004i005p00195

Gjerloev, J. (2012). The supermag data processing technique. *Journal of Geophysical Research*. doi: 10.1029/2012ja017683

Glocer, A., Knipp, D. J., Welling, D. T., Chappell, C. R., Toth, G., Fok, M.-C., … Mouikis, C. G. (2020). A Case Study on the Origin of Near-Earth Plasma. *Journal of Geophysical Research*, *125*(11). (MAG ID: 3092127848 S2ID: 43093870f71cf9874766a4d10d8f8427d006e551) doi: 10.1029/2020ja028205

H. Zhang, J. Lu, & M. Wang. (2023). Energy transfer across magnetopause under dawn–dusk IMFs. *Scientific Reports*. (S2ID:

0b05fcadd7b55c510bf683b313dcef261c659c14) doi: 10.1038/s41598-023-34082-2

Hoilijoki, S., Souza, V. M., Walsh, B., Janhunen, P., & Palmroth, M. (2014, June). Magnetopause reconnection and energy conversion as influenced by the dipole tilt and the IMF Bx. *Journal of Geophysical Research*, *119*(6), 4484–4494. (MAG ID: 2068425892 S2ID: 2ef15c9979783f5d50f964286bfbbeed911e4978) doi: 10.1002/2013ja019693

Imber, S. M., Milan, S., & Hubert, B. (2007, July). Observations of significant flux closure by dual lobe reconnection. *Annales Geophysicae*, *25*(7), 1617–1627. (MAG ID: 2102759485 S2ID: e98098aa3a7aaca9755c5c6f878132c5a8ac62f4) doi: 10.5194/angeo-25-1617-2007

Laitinen, T., Palmroth, M., Pulkkinen, T., Janhunen, P., & Koskinen, H. E. (2007). Continuous reconnection line and pressure-dependent energy conversion on the magnetopause in a global mhd model. *Journal of Geophysical Research: Space Physics*, *112*(A11).

Lavraud, B., Lavraud, B., Fedorov, A., Budnik, E., Budnik, E., Thomsen, M. F., … Balogh, A. (2005, February). High-altitude cusp flow dependence on IMF orientation: A 3-year Cluster statistical study. *Journal of Geophysical Research*, *110*. (MAG ID: 2014153421 S2ID: 3baa2b61bf45eccd0d4135e6729aaca65e1fa738) doi: 10.1029/2004ja010804

Lockwood, M., Smith, M., & Smith, M. F. (1992, October). The variation of reconnection rate at the dayside magnetopause and cusp ion precipitation. *Journal of Geophysical Research*, *97*, 14841–14847. (MAG ID: 2057582708 S2ID: d663868749ef8c37a86a44c6d4425ab981c05800) doi: 10.1029/92ja01261

Lu, J., Zhang, H., Wang, M., Kabin, K., Zhou, Y., & Li, J. (2021). Energy transfer across the magnetopause under radial imf conditions. *The Astrophysical Journal*, *920*(1), 52.

Mays, M. L., Horton, W., Spencer, E., & Kozyra, J. U. (2009, July). Real-time predictions of geomagnetic storms and substorms: Use of the Solar Wind Magnetosphere-Ionosphere System model. *Space Weather-the International Journal of Research and Applications*, *7*(7), 07001. (MAG ID: 2101176004 S2ID: 46ac1c8968e75c7454fcfae60b16771d824a0517) doi: 10.1029/2008sw000459

Milan, S., Milan, S. E., Carter, J. A., Carter, J. A., Bower, G., Imber, S. M., … Hubert, B. (2020, October). Dual-Lobe Reconnection and Horse-Collar Auroras. *Journal of Geophysical Research*, *125*(10). (MAG ID: 3048850697 S2ID: cc65b1d3429a850af95fd835f9254dda4dffb325) doi: 10.1029/2020ja028567

Mish, W. H., Green, J. L., Reph, M. G., & Peredo, M. (1995). Istp science data systems and products. *Space Science Reviews*, *71*(1), 815–877. Retrieved from `https://doi.org/10.1007/BF00751352` doi: 10.1007/BF00751352

Mukhopadhyay, A., Welling, D. T., Liemohn, M. W., Ridley, A. J., Chakraborty, S., & Anderson, B. J. (2020). conductance model for extreme events impact of auroral conductance on space weather forecasts. *Social Work*. (ARXIV_ID: 2008.12276 MAG ID: 3088886888 S2ID: fed95313c4472d29820cf3a356f07e3e699b270d) doi: 10.1002/essoar.10503207.1

Newell, P. T., Sotirelis, T., Sotirelis, T., Liou, K., Meng, C.-I., Rich, F. J., & Rich, F. J. (2007). A nearly universal solar wind-magnetosphere coupling function inferred from 10 magnetospheric state variables. *Journal of Geophysical Research*. doi: 10.1029/2006ja012015

Palmroth, M., Ganse, U., Pfau-Kempf, Y., Battarbee, M., Turc, L., Brito, T., … von Alfthan, S. (2018, August). Vlasov methods in space physics and astrophysics. *Living Reviews in Computational Astrophysics*, *4*(1), 1. doi: 10.1007/s41115-018-0003-2

Palmroth, M., Pulkkinen, T., Janhunen, P., & Wu, C.-C. (2003). Stormtime energy transfer in global MHD simulation. , *108*, 1048. doi: 101029/2002JA009446

Pitout, F., Pitout, F., Bogdanova, Y., & Y.V. Bogdanova. (2021, September). The polar cusp seen by Cluster. *Journal of Geophysical Research*, *126*(9). (MAG ID: 3198503423 S2ID: e32590a3857463156fbaf367fe806ad7df7760a5) doi: 10.1029/2021ja029582

Pulkkinen, T. (2007). Space weather: Terrestrial perspective. *Living Reviews in Solar Physics*, *4*(1), 1. Retrieved from `https://doi.org/10.12942/lrsp-2007-1` doi: 10.12942/lrsp-2007-1

Ridley, A. J., Gombosi, T. I., Sokolov, I. V., Toth, G., Knipp, D. J., & Welling, D. T. (2010, August). Numerical considerations in simulating the global magnetosphere. *Annales Geophysicae*, *28*(8), 1589–1614. (MAG ID: 2090366793 S2ID: a8f87999528ca9c5c01cd68b7cf09fa21602dadf) doi: 10.5194/angeo-28-1589-2010

Russell, C. (1972). The configuration of the magnetosphere, critical problems in magnetospheric physics er dyer, 1–16, iucstp sec. *Natl. Acad. of Sci., Washington, DC*.

Shidi, Q. A. A., Pulkkinen, T., Toth, G., A. Brenner, Zou, S., & Gjerloev, J. (2022, October). A Large Simulation Set of Geomagnetic Storms—Can Simulations Predict Ground Magnetometer Station Observations of Magnetic Field Perturbations? *Space Weather-the International Journal of Research and Applications*, *20*(11). (MAG ID: 4307893952 S2ID: 077de025409cd06d56c6f11d073aacaed1909242) doi: 10.1029/2022sw003049

Siscoe, G. L., & Huang, T. S. (1985). Polar cap inflation and deflation. *Journal of Geophysical Research*. doi: 10.1029/ja090ia01p00543

Toth, G., van der Holst, B., van der Holst, B., Sokolov, I. V., De Zeeuw, D. L., Darren L. De Zeeuw, ... Opher, M. (2012, February). Adaptive numerical algorithms in space weather modeling. *Journal of Computational Physics*, *231*(3), 870–903. (MAG ID: 1964419747) doi: 10.1016/j.jcp.2011.02.006

Welling, D. T., & Liemohn, M. W. (2014, April). Outflow in global magnetohydrodynamics as a function of a passive inner boundary source. *Journal of Geophysical Research*, *119*(4), 2691–2705. (MAG ID: 2059015120) doi: 10.1002/2013ja019374

Xu, S., Liemohn, M. W., Dong, C., Mitchell, D. L., Bougher, S. W., & Ma, Y. (2016, July). Pressure and ion composition boundaries at Mars. *Journal of Geophysical Research*, *121*(7), 6417–6429. (MAG ID: 2460334105 S2ID: 3de377f44554d5d18464a131bb726541730a1253) doi: 10.1002/2016ja022644

Zhang, Y., Paxton, L. J., Schaefer, R. K., & Swartz, W. H. (2022, September). Thermospheric Conditions Associated With the Loss of 40 Starlink Satellites. *Space Weather-the International Journal of Research and Applications*, *20*(10). (MAG ID: 4296042710 S2ID: c14606a3acf0c1a7abdf075d1b266fb3bae31df9) doi: 10.1029/2022sw003168

Table 1: Time integrals over the storm main phase of the hydrodynamic energy flux, Poynting flux, and total energy flux.

	Energy $[PJ]$	$\int H dt$	$\int S dt$	$\int K dt$
1	Lobes→Sheath	+4.67	–97.28	–92.61
2a	Closed→Lobes (day)	+11.20	+58.82	+70.01
2b	Closed→Lobes (night)	–3.45	–153.12	–156.56
3	Lobes→Inner	–1.72	–15.34	–17.06
4	Lobes→TailCut	+7.01	+3.94	+10.96
5	Closed→Sheath	+46.62	+14.57	+61.19
6	Closed→TailCut	–10.57	–6.21	–16.79
7	Closed→Inner	+12.69	+40.48	+27.80

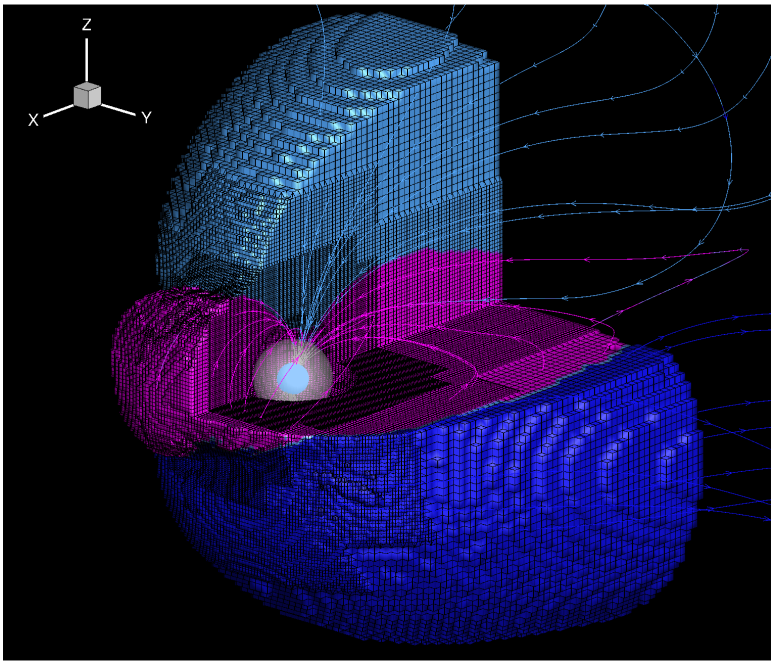

Figure 1: Cut-away of the 3D magnetosphere showing various regions and the grid resolution of the simulation. Magenta: Closed field line region, Blue: Lobes, Grey: Inner boundary surface.

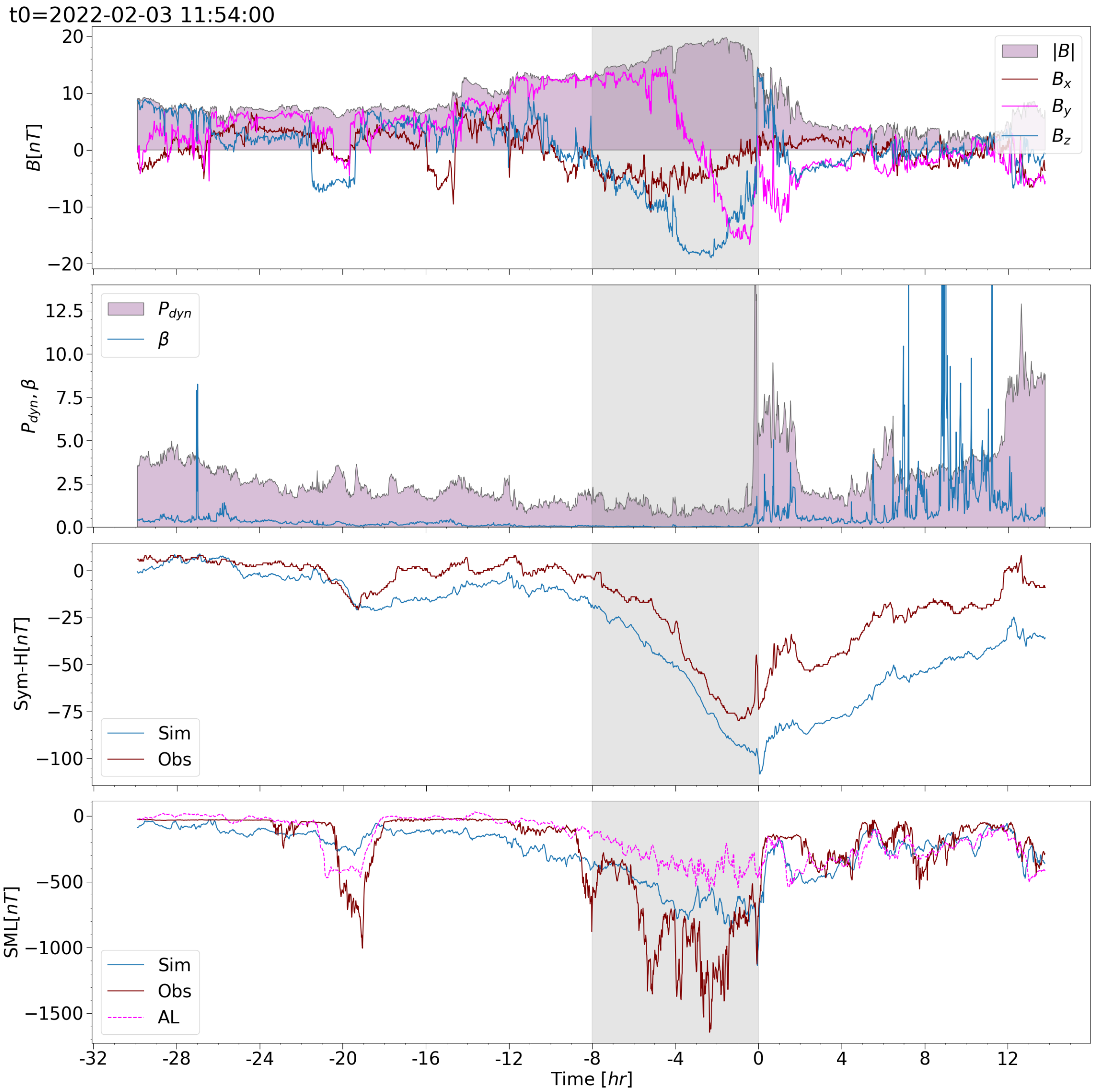

Figure 2: Panels from top to bottom: The IMF components and magnetic field magnitude; Solar wind dynamic pressure (shaded) and plasma β (blue); Observed (red) and simulation (blue) SYM-H index; and Observed (red) and simulation (blue) SML index. The simulation AL index (magenta) is shown for comparison.

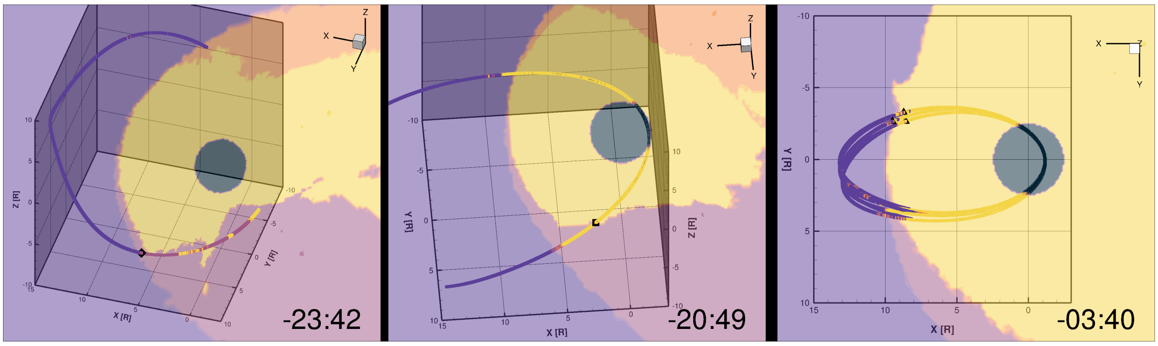

Figure 3: Orbit plane slices showing the trajectories within the simulation domain with contour of the virtual satellite status. Cluster4 (left), MMS (center), Themis (right). Color coding shows the status variables closed (yellow), Open-North (orange), Open-South (maroon), Open-Solar Wind (purple), Outside simulation domain (black).

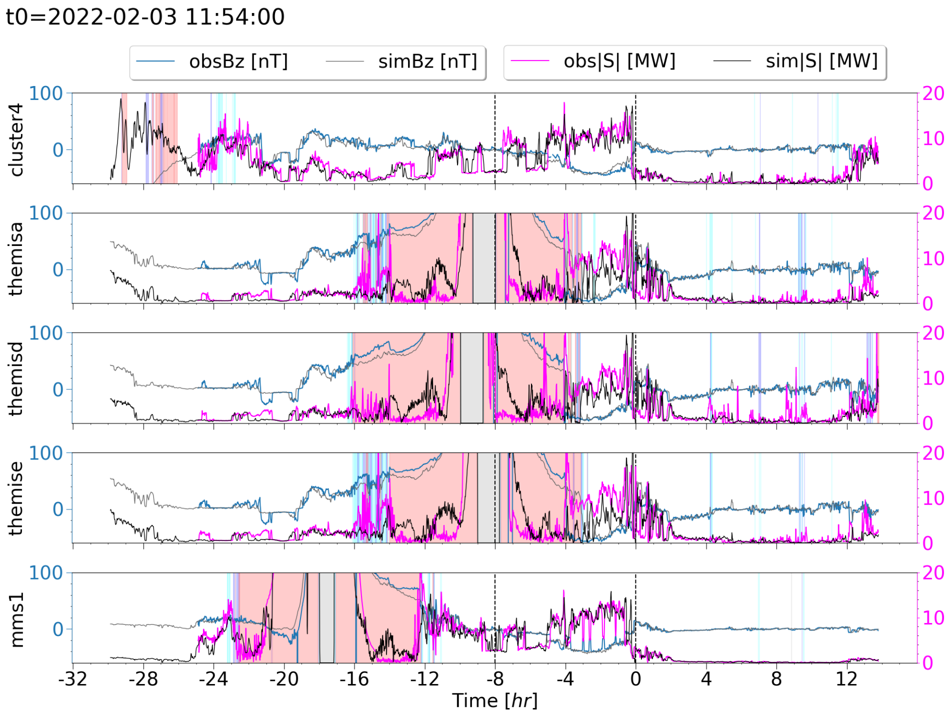

(a)

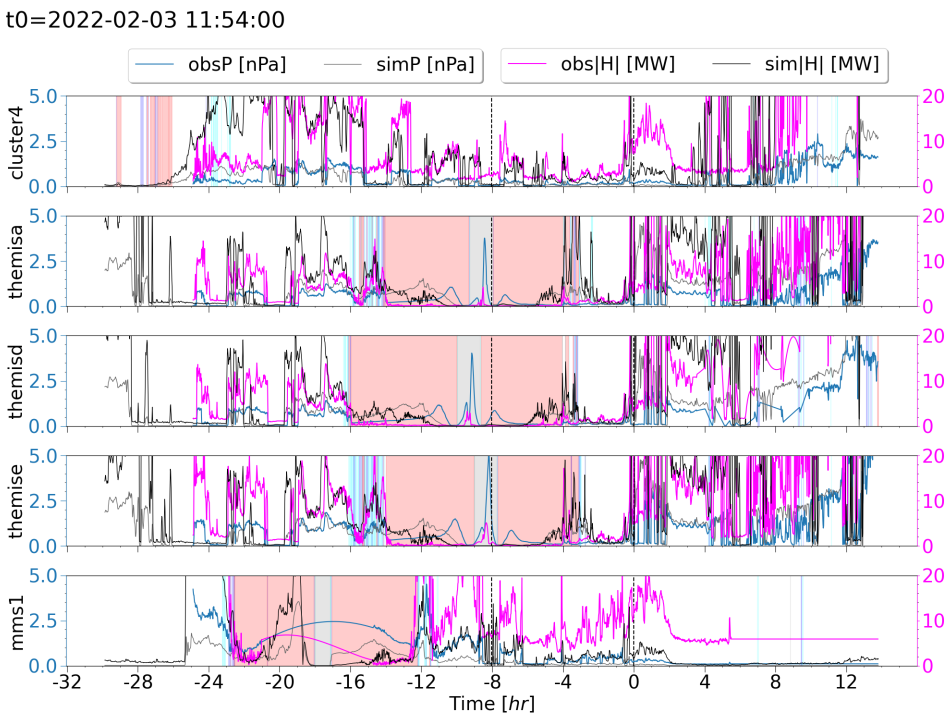

(b)

Figure 4: (a) (Left vertical axis) Magnetic field B_Z time series from Cluster-4, Themis-A, Themis-D, Themis-E, and MMS-1 spacecraft (blue) and simulated B_Z at the satellite locations (gray). (Right vertical axis) The observed (magenta) and simulated (black) Poynting flux **S** defined in equation 2. (b) (Left vertical axis) Plasma total pressure $P = P_{th} + P_{dyn}$ time series from Cluster-4, Themis-A, Themis-D, Themis-E, and MMS-1 spacecraft (blue) and simulated P at the satellite locations (gray). (Right vertical axis) The observed (magenta) and simulated (black) hydrodynamic energy flux **H** defined in equation 1. Vertical shading indicates virtual satellite location status within the open (blue), closed (red), magnetosheath or solar wind (white).

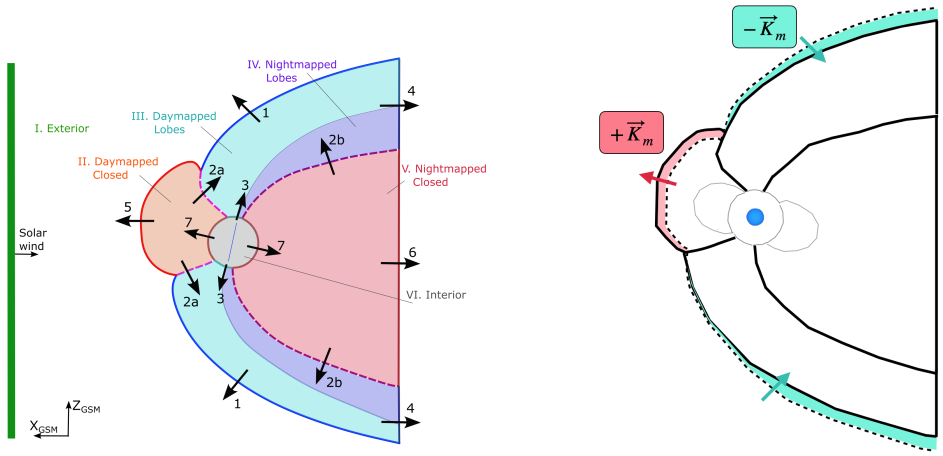

(a) Surface fluxes w/ reference vectors

(b) Motion flux

Figure 5: (a) Diagram of the magnetospheric cross section in GSM $X - Z$ plane showing reference vectors for energy fluxes between the sheath and lobes (1), lobes and closed $(2a, 2b)$, closed and sheath (5) as well as magnetic flux transport at the inner boundary $(3, 7)$, and through the tail cut off $(4, 6)$. (b) Illustration of boundary motion contribution to surface flux. Between a time t_0 (solid lines) and t_1 (dashed lines), flux is transported away from the dayside and towards the lobes as the volumes contract and expand.

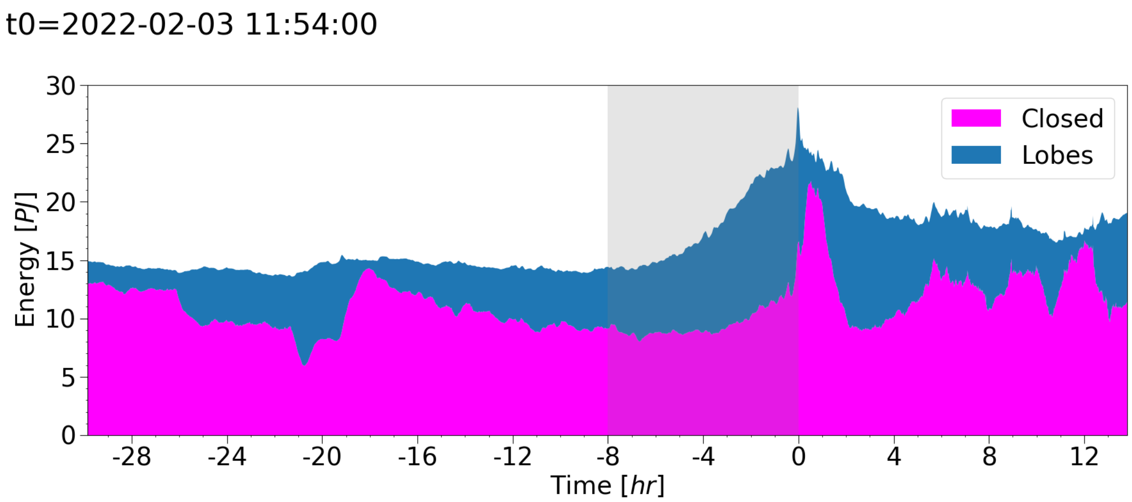

Figure 6: Time series of energy content in the open lobes (blue) and closed magnetosphere (magenta) regions in the magnetosphere in a stackplot format. The vertical shaded portion indicates the storm main phase.

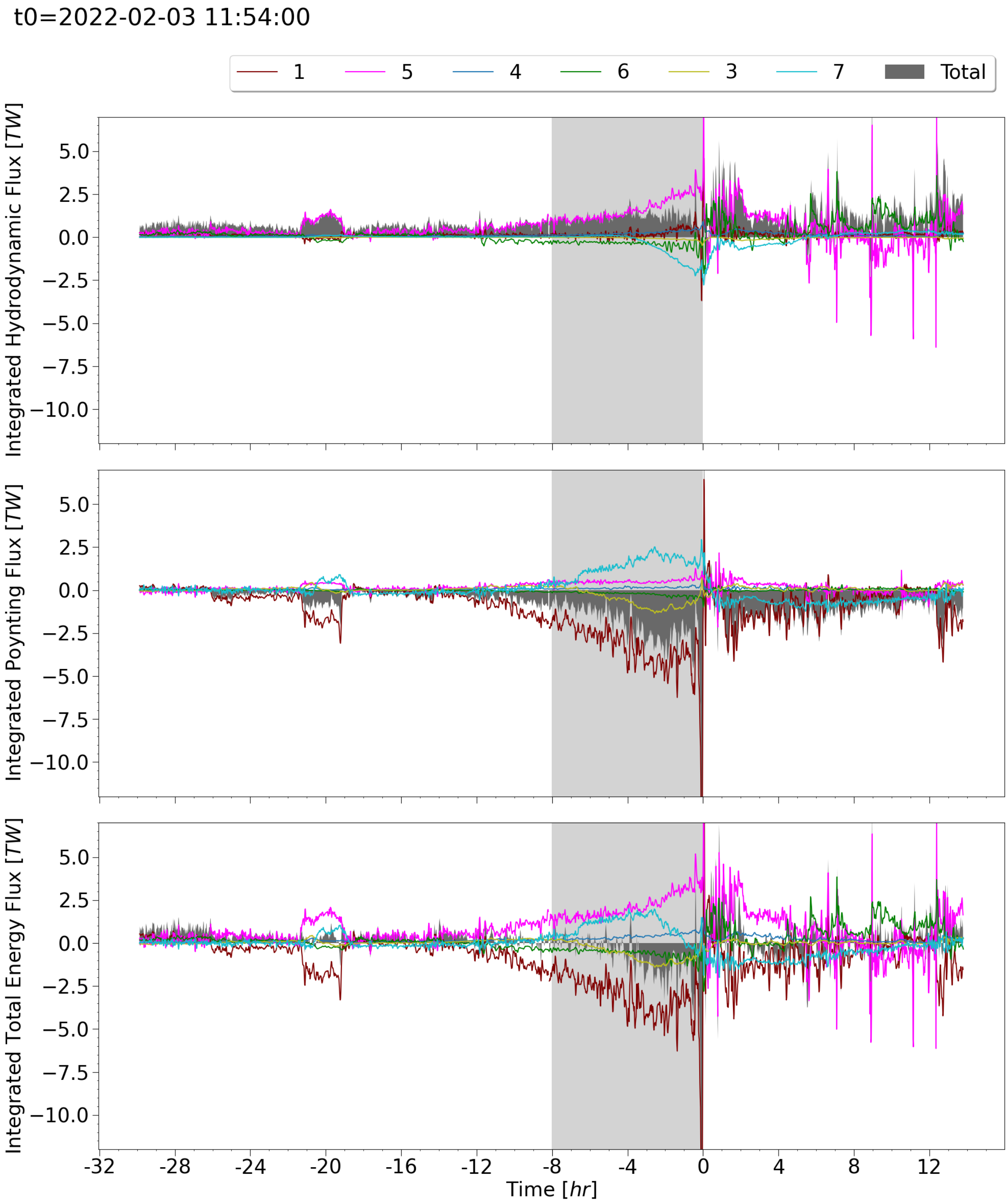

Figure 7: Time series of spatially integrated energy flux values over magnetospheric external interfaces: 1 open tail lobes – magnetosheath, 5 closed field region – magnetosheath, 4 open tail lobes – tail cutoff, 6 closed field region – tail cutoff, 3 open tail lobes – inner boundary (ionosphere), 4 closed field region – inner boundary (ionosphere). Top panel gives the hydrodynamic energy flux, middle panel gives the Poynting flux, and the bottom panel gives the total energy flux. Solid gray shading indicates the summed total of all individual contributions. Negative (positive) values indicate energy increase (decrease) in the magnetospheric volume between the inner boundary and the magnetopause.

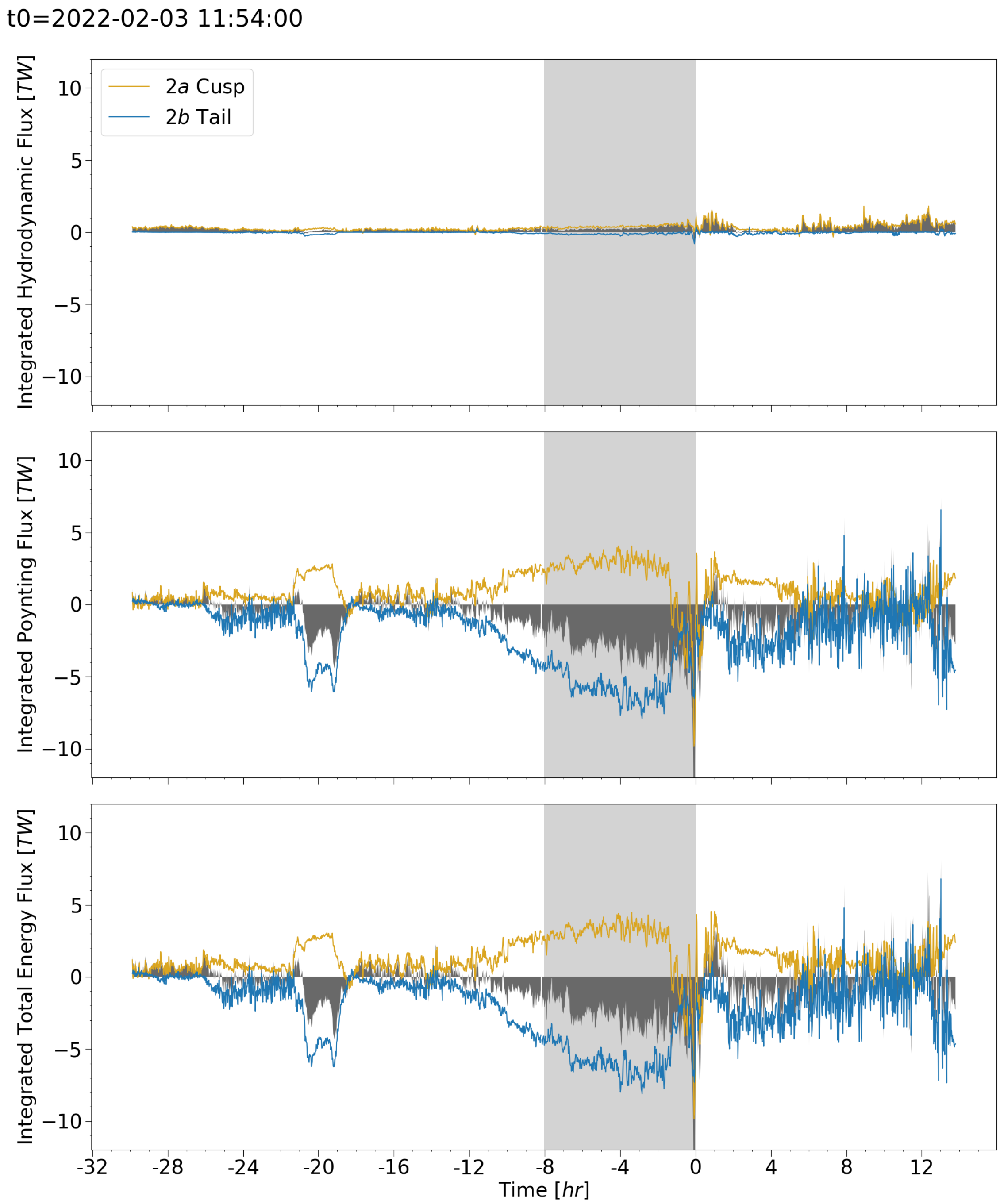

Figure 8: Time series of spatially integrated flux values over magnetospheric internal interfaces: 2a dayside closed field region – open tail lobes (cusp), 2b nightside closed field region – open tail lobes (tail). Top panel gives the hydrodynamic flux, middle panel gives the Poynting flux, and the bottom panel gives the total energy flux. Solid gray shading indicates the summed total of all individual contributions. Negative (positive) values indicate energy increase (decrease) in the closed field region, the opposite is true for the lobes.

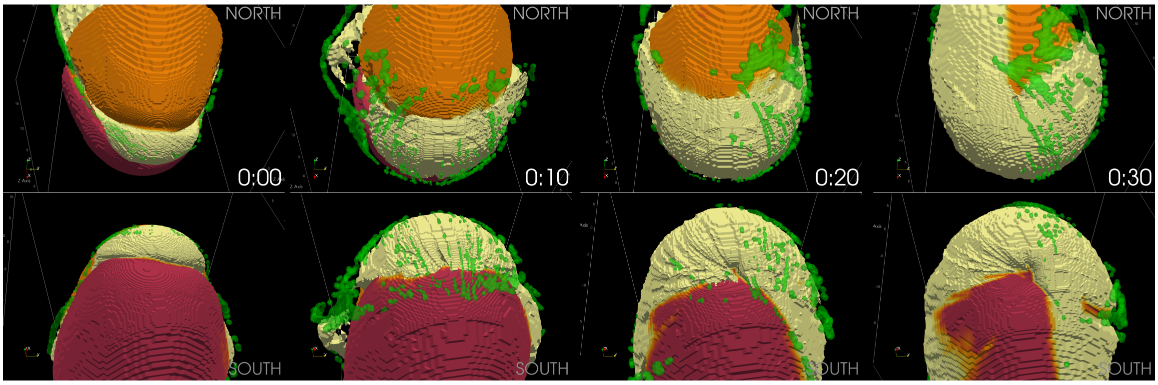

Figure 9: Snapshots of simulated magnetopause surface colored by Status (Yellow - closed, Orange - open north, Red - open south). Two views show the northern and southern cusp regions. The green iso-surfaces indicate neighborhoods around four field junctions (cells with status open-open,open-closed,closed-open, and closed-closed all adjacent), which indicate possible magnetic reconnection locations. Snapshot at T=0 is taken just after IMF northward turning and at three consecutive times 10-min apart, showing a single dayside X-line morphing and dual lobe reconnection occurring.

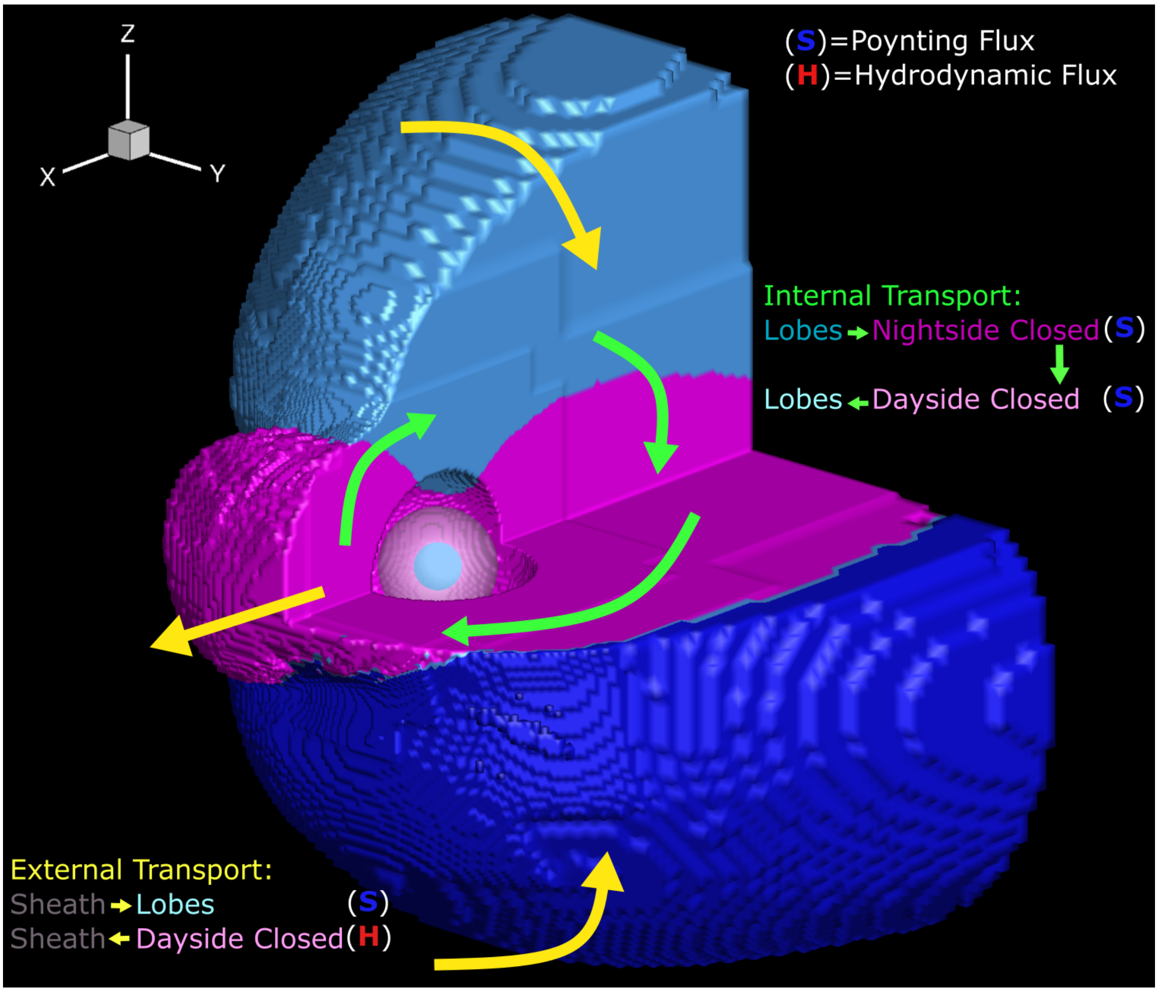

Figure 10: Summary of energy transport pathways. During most of main phase both an internal and external energy pathway were found following the corresponding arrows.